ARMY RESEARCH LABORATORY

Low Pressure Chemical Vapor Deposition (LPCVD) Graphene Growth Study and Raman Characterization

by Barbara M. Nichols

ARL-TR-6751 **December 2013**

NOTICES

Disclaimers

The findings in this report are not to be construed as an official Department of the Army position unless so designated by other authorized documents.

Citation of manufacturer's or trade names does not constitute an official endorsement or approval of the use thereof.

Destroy this report when it is no longer needed. Do not return it to the originator.

Army Research Laboratory
Adelphi, MD 20783-1197

ARL-TR-6751 **December 2013**

Low Pressure Chemical Vapor Deposition (LPCVD) Graphene Growth Study and Raman Characterization

Barbara M. Nichols
Sensors and Electron Devices Directorate, ARL

REPORT DOCUMENTATION PAGE

Form Approved
OMB No. 0704-0188

1. **REPORT DATE** *(DD-MM-YYYY)*	**2. REPORT TYPE**	**3. DATES COVERED (From - To)**
December 2013	Final	June 2012 to June 2013

4. TITLE AND SUBTITLE
Low-Pressure Chemical Vapor (LPCVD) Graphene Growth Study and Raman Characterization

5a. CONTRACT NUMBER

5b. GRANT NUMBER

5c. PROGRAM ELEMENT NUMBER

6. AUTHOR(S)
Barbara M. Nichols

5d. PROJECT NUMBER

5e. TASK NUMBER

5f. WORK UNIT NUMBER

7. PERFORMING ORGANIZATION NAME(S) AND ADDRESS(ES)
U.S. Army Research Laboratory
ATTN: RDRL-SER-L
2800 Powder Mill Road
Adelphi MD 20783-1197

8. PERFORMING ORGANIZATION REPORT NUMBER
ARL-TR-6751

9. SPONSORING/MONITORING AGENCY NAME(S) AND ADDRESS(ES)

10. SPONSOR/MONITOR'S ACRONYM(S)

11. SPONSOR/MONITOR'S REPORT NUMBER(S)

12. DISTRIBUTION/AVAILABILITY STATEMENT
Approved for public release; distribution unlimited.

13. SUPPLEMENTARY NOTES

14. ABSTRACT
Details of the Raman spectroscopy analysis of graphene films deposited for a growth study is discussed. Low pressure chemical vapor deposition was utilized to grow graphene layers onto copper foil substrates. For this study, the hydrogen-to-methane (H_2/CH_4) gas ratio used for the growths was varied from 20 to 200. Once transferred to patterned SiO_2/Si substrates, the graphene layers were characterized by Raman spectroscopy. Using the characteristic Raman peaks for graphene and silicon, maps of the integrated area ratio of the G and Si bands (A_G/A_{Si}), peak intensity ratio of the G' and G bands ($I_{G'}/I_G$), and the G' peak full-width−half-maximum (FWHM) were used to identify the number of layers and stacking orientation. Distinction between single-layer, Bernal-stacked bilayer, and turbostratic (or disoriented) bilayer graphene was made using this analysis. For the graphene deposited in this study, 100% monolayer graphene coverage was not achieved. All growths exhibited small areas of bilayer graphene. Although no correlation between the H_2/CH_4 gas ratio and the bilayer composition and/or stacking configuration was found, an increase in the size of the bilayer graphene was observed as the H_2/CH_4 gas ratio increased. This methodology is useful for relating graphene growth parameters to Raman properties.

15. SUBJECT TERMS
Graphene, chemical vapor deposition

16. SECURITY CLASSIFICATION OF:			**17. LIMITATION OF ABSTRACT**	**18. NUMBER OF PAGES**	**19a. NAME OF RESPONSIBLE PERSON**
a. REPORT	**b. ABSTRACT**	**c. THIS PAGE**			Barbara M. Nichols
Unclassified	Unclassified	Unclassified	UU	22	**19b. TELEPHONE NUMBER** (*Include area code*) (301) 394-0602

Contents

List of Figures

List of Tables

1. Introduction

Graphene is a monolayer material comprised of sp^2 bonded carbon atoms that form a honeycomb-like lattice structure. Because it is only one atom thick, it is the prototypical two-dimensional material and, as such, exhibits unique physical properties, including a high intrinsic mobility (200,000 cm^2/Vs) (*1*) and a constant optical absorption of 2.3% per layer over a wide spectral range (*2*). Graphene was first isolated physically by the mechanical exfoliation method (*3*); however, recent efforts have focused on graphene synthesis by conventional methods, such as chemical vapor deposition (CVD) and ultrahigh vacuum, high temperature annealing (i.e., epitaxial graphene from SiC) (*4, 5*). CVD, in particular, is a promising growth technique because of the ability to deposit large areas of graphene on inexpensive, transition metal materials (e.g., nickel and copper).

Graphene growth on nickel (Ni) and copper (Cu) metals exhibit two distinctly different mechanisms (*6*). At high temperatures (~1000 °C), carbon atoms dissolve into nickel up to ~1 atomic percent (at. %) (*7*). Then, as the temperature is lowered, the carbon atoms precipitate out of the nickel and form graphene on the Ni surface. Conversely, carbon only has a 0.001 at. % solubility in Cu and hardly any carbon atoms are dissolved in the metal (*7*). Graphene is formed by catalytic decomposition on the copper surface, and once the surface is covered, graphene formation is terminated. The different grown mechanisms generally explain why single-layer graphene (SLG) can be achieved on Cu; whereas, multilayer growth is typically found on Ni. Because of the desire to produce uniform single graphene layers, Cu has become the preferred substrate for CVD graphene growth.

Many parameters influence the growth of graphene on copper. These include pressure, gas flow rates, temperature, and the ratio between the carrier and carbon feedstock gases (i.e., hydrogen and methane) used for growth (*8–10*). In particular, hydrogen is known to play an important dual role in the growth of graphene by CVD methods. First, it acts as an activator for the surface bound carbon to form graphene; however, it can also serve as an etching agent, which helps control the size and shape of the graphene domains (*8*). CVD growth conditions have also been shown to determine the graphene grain size, which in turn have been correlated to electrical performance. Large grain graphene has produced higher mobility values (20,000 versus 1200 cm^2/Vs) and lower sheet resistances (20 versus 920 Ω/□) than small-grained graphene on SiO_2 and hexagonal boron nitride (h-BN) (*11*). Larger grain graphene is typically grown at small hydrogen-to-methane (H_2/CH_4) ratio values (~1) and lower pressures (<500 mTorr) (*11, 8*); whereas, higher H_2/CH_4 ratio values (e.g., 40) tend to promote the formation of bilayer graphene (*9*).

In this report, we discuss the Raman spectroscopy results of a study varying the H_2/CH_4 gas flow ratio for graphene grown by low pressure chemical vapor deposition (LPCVD). First, the

grapene was grown on copper foils and transferred onto grid-patterned SiO_2/Si substrates. After transfer, the samples were characterized by Raman spectroscopy. Analysis of the Raman data showed the coexistence of both single-layer and double-layer (or bilayer) graphene over areas as large as 80 × 80 μm. Details of the analysis will be given as well as a discussion of the Raman charactertistics that distinguish ordered (AB or Bernal-stacked) and disoriented (or turbostratic) bilayer graphene (BLG).

2. Experimental Procedure

Graphene was synthesized by LPCVD using hydrogen and methane as the carrier and carbon feedstock gases. Copper foils (99.8% pure), approximately 25 and 125 μm thick, were cleaned with acetic acid, acetone, and isopropanol, and loaded into the furnace. The furnace was pumped down to a base pressure less than 0.5 Torr and then heated to 1000 °C in 100 sccm of H_2. Once the furnace reached temperature, the copper foils were annealed for 30 min under flowing H_2. Next, CH_4 was metered into the furnace with the throttle valve open 100% to the mechanical vacuum pump. Growth pressure ranged between 0.5 and 0.6 Torr. After 20 min, the methane flow was stopped, and the furnace was cooled to room temperature under 100 sccm of H_2. For these experiments, the H_2/CH_4 gas flow ratio was varied by keeping the hydrogen flow fixed at 100 sccm and changing the methane flow rate. The methane flow rate was varied from 0.5 to 5 sccm. A summary of the growth conditions can be seen in table 1. After growth, the samples were examined with a scanning electron microscope (SEM).

Table 1. Summary of the LPCVD parameters for the H_2/CH_4 graphene growth study.

Sample	H_2 Flow (sccm)	CH_4 Flow (sccm)	H_2/CH_4 Ratio	Time (min)	Pressure (Torr)	Temperature (°C)
LPC065	100	5	20	20	0.56	1000
LPC066	100	2	50	20	0.55	1000
LPC067	100	3	33	20	0.59	1000
LPC068	100	1	100	20	0.55	1000
LPC069	100	0.5	200	20	0.55	1000
LPC070	100	4	25	20	0.56	1000

After growth, the graphene was transferred to patterned SiO_2/Si substrates via a wet chemical etching process of the copper foil. First, a protective layer of poly(methyl methacrylate) (PMMA) was spun onto the graphene using either 495 PMMA A4 (4% PMMA in anisole), 495 PMMA A8 (8% PMMA in anisole), or a combination of the two and baked at 150 °C for 90 s. Next, the unprotected side of the copper foil was exposed to an oxygen plasma (power = 50 W, O_2 flow = 200 sccm, pressure = 0.5 Torr) to remove the backside graphene layer. The copper foil was then chemically etched away using a commercial ferric chloride based etchant (Transene CE-100), followed by a 10% HCl in H_2O etch to remove any particulate residue from the copper

etchant. After each etch step, the PMMA/graphene was floated on water baths to immediately stop any chemical reactions. The floating PMMA/graphene was then placed onto the substrate and baked on a hot plate between 50 and 75 °C for 7–10 min to drive away excess water between the substrate and the PMMA/graphene layer. The patterned substrates were designed and fabricated at the U.S. Army Research Laboratory (ARL) as a marker grid to locate areas on the substrate. The grid structure was patterned using standard photolithography techniques and buffer oxide etched into the silicon dioxide approximately 100–150 nm deep (see figure 1). The grid was visible underneath the graphene. Removal of the PMMA layer was performed by soaking the sample in chloroform for 90 min, followed by an ispropanol/acetone/isopropanol rinsing. Prior to the chloroform soaking, the sample was baked on a hot plate (~200 °C) for 5 min to dewrinkle/smooth the PMMA/graphene on the substrate. The samples were later thermal annealed at 350 °C for 2 h in a mixed hydrogen/argon atmosphere to further remove any PMMA residue found on the surface.

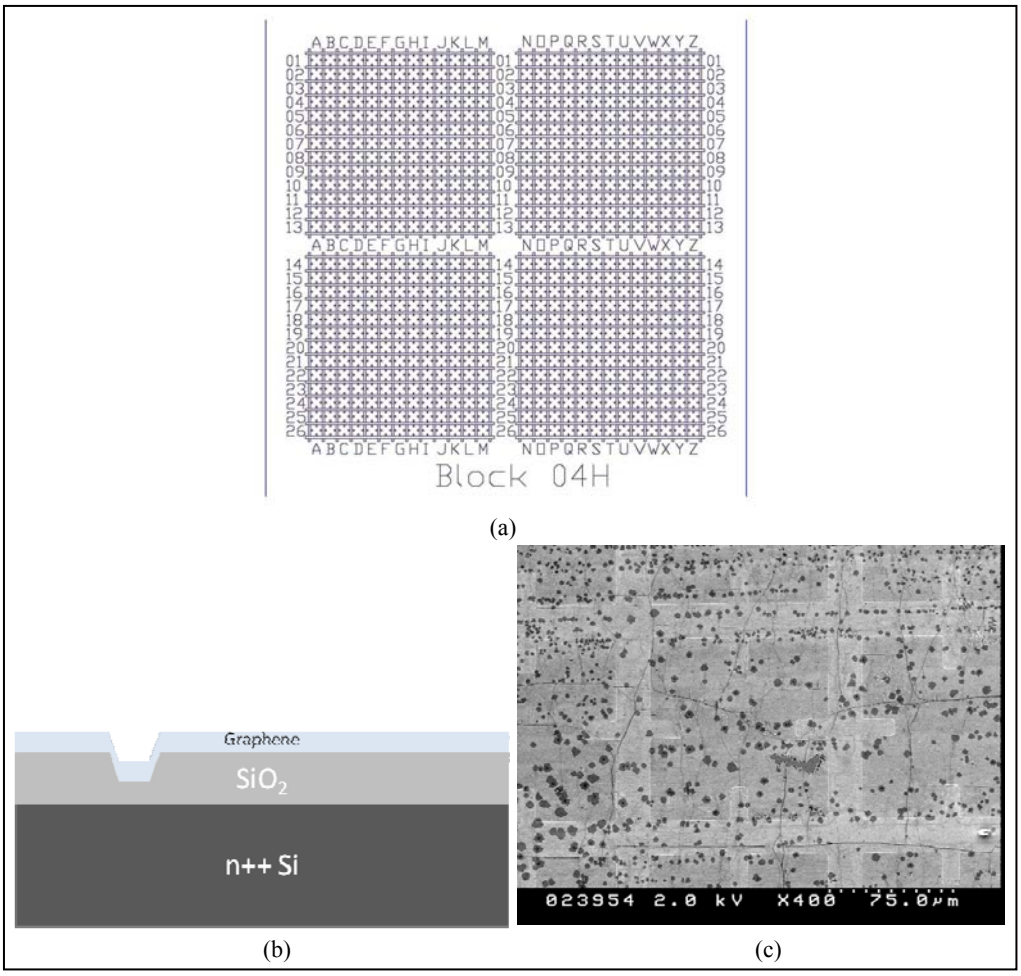

Figure 1. (a) Drawing of the grid pattern etched into SiO_2/Si substrates for identification purposes, (b) Cross-sectional drawing of the transferred graphene samples, and (c) a SEM image of graphene transferred onto a patterned substrate (LPC068B1TCA – H_2 = 100 sccm, CH_4 = 1 sccm).

Raman spectroscopy measurements were performed to characterize the graphene after transfer, after PMMA removal via chloroform, and after thermal annealing. A WITec alpha300RA confocal Raman microscope (CRM) allowed for the acquisition of individual Raman spectrum over large areas (up to 80 × 80 µm) with submicron spacing. The CRM was operated with a laser wavelength of 532 nm, ~1.5 mW power at the sample, and a 600 grooves/mm grating. This capability produced detailed views of the transferred films that revealed information about the number of graphene layers and other features, such as wrinkles and folds. Because of the patterned silicon dioxide substrates, the exact graphene location was scanned after the three steps mentioned above to specifically detail if/how the PMMA removal steps affected the graphene. The Raman spectroscopy data was analyzed using the Lorentz peak fitting approximation for the

characteristic graphene peaks – G' peak at ~2670 cm−1, G peak at ~1580 cm−1 and D peak at ~1350 cm−1, as well as the Si peak at ~520 cm−1. Once fitted, the individual peak features, such as full-width−half-maximum (FWHM), peak height, and peak position, could be plotted as maps, revealing structural information about the graphene, including the number of layers and structural stacking configurations.

3. Results and Discussion

3.1 Raman Characterization

The results of a Raman mapping scan of one transferred graphene growth can be seen in figure 2. Figure 2a shows a 100 × 100 μm optical image (taken under a green filter) of a transferred graphene film (LPC069B1TC). The optical image shows a large monochromatic field with multiple darker patches and lines. The four lighter rectangles in the figure are the etched SiO_2 trenches, which are covered by the graphene film. Using the maps developed from the Raman spectra (1 individual spectra was collected per pixel), one can correlate features in the optical image with those observed in the Raman maps. The location of bright areas seen in the A_G/A_{Si} (peak area ratio between the G and Si peaks) map in figure 2b correspond to the dark patches in the optical image, revealing that the bright locations are composed of two or more graphene layers. Aside from the etched trenches, dark areas indicate the presence of no graphene, likely due to a slight rip or tear in the otherwise continuous graphene film. A map of the G' peak FWHM can be found in figure 2c. It has been shown that the graphene G' peak is extremely sensitive to both the number and stacking of bilayer and few layer graphene (*12*). Wider G' peaks have been shown to belong to energetically favored stacking in multiple graphene layered materials, such as AB (Bernal-stacked) bilayer or ABC/ABA trilayer; whereas, turbostratically oriented layers (layers randomly rotated with respect to one another) typically have narrower widths than single-layer graphene (*9*). In figure 2c, the areas composed of two or more layers have FWHM values that are either smaller (28–32 cm^{-1}) or larger (>45 cm^{-1}) than the single-layer median value of 36 cm^{-1}. The third important feature for graphene is the peak height or intensity ratio between the G' and G peaks, denoted as $I_{G'}/I_G$ (see figure 2d). Early on, the peak intensity ratio $I_{G'}/I_G$ was used as an indicator of graphene layer number and with recent understanding, it can also be used to infer stacking order (*9*). The map has a median intensity ratio of 1.75, which is near but less than the $I_{G'}/I_G$ value of 2, which has been used as an indicator of single-layer graphene. However, the map also reveals areas with significantly higher (~2.6) and lower (~0.8) values than the median. Using these three variable maps, A_G/A_{Si}, G' FWHM, and $I_{G'}/I_G$, one can differentiate areas of the graphene by both layer count and stacking configuration, which is particularly important because the electrical properties of graphene strongly depend upon these variables.

Figure 3 shows a map identifying the graphene areas observed in figure 2. An approach similar to reference 13 was taken to develop the map. The majority of the scanned area is composed of single-layer graphene; however, both Bernal-stacked and turbostratic bilayer areas have been identified. The graphene areas over the etched trenches were excluded from the compositional identification because the low Raman spectra intensity at these areas made it difficult to perform peak fitting (and thus are colored gray in figure 3a). The black areas in the image are locations where the composition could not be determined because they did not fit the general guidelines discussed above. These locations are primarily composed of the wrinkles/folds observed in the image. Because the folds/wrinkles are formed as a result of thermal expansion differences between the graphene and copper during the cool down phase of the growth or from the transfer process, it is expected that they could exhibit properties different from AB-stacked or turbostratic BLG (*4*). There are also bilayer areas where the stacking configuration could not be determined. These areas most likely have G'FWHM or $I_{G'}/I_G$ values that typically mark transition areas between different stacking configurations or layers. While every pixel of the map was not able to be definitively identified, a large majority were identified and the results can be used to give a composition summary of the scanned area. Based on the analysis, the scan area found in figures 2 and 3 is composed of 88% SLG, 3% turbostratic BLG (T-BLG) and 1.9% Bernal-stacked BLG (AB-BLG). The analysis also indicates that 0.5% of the scanned area is composed on trilayer graphene. Wrinkles and other unidentifiable areas make up 6.5%.

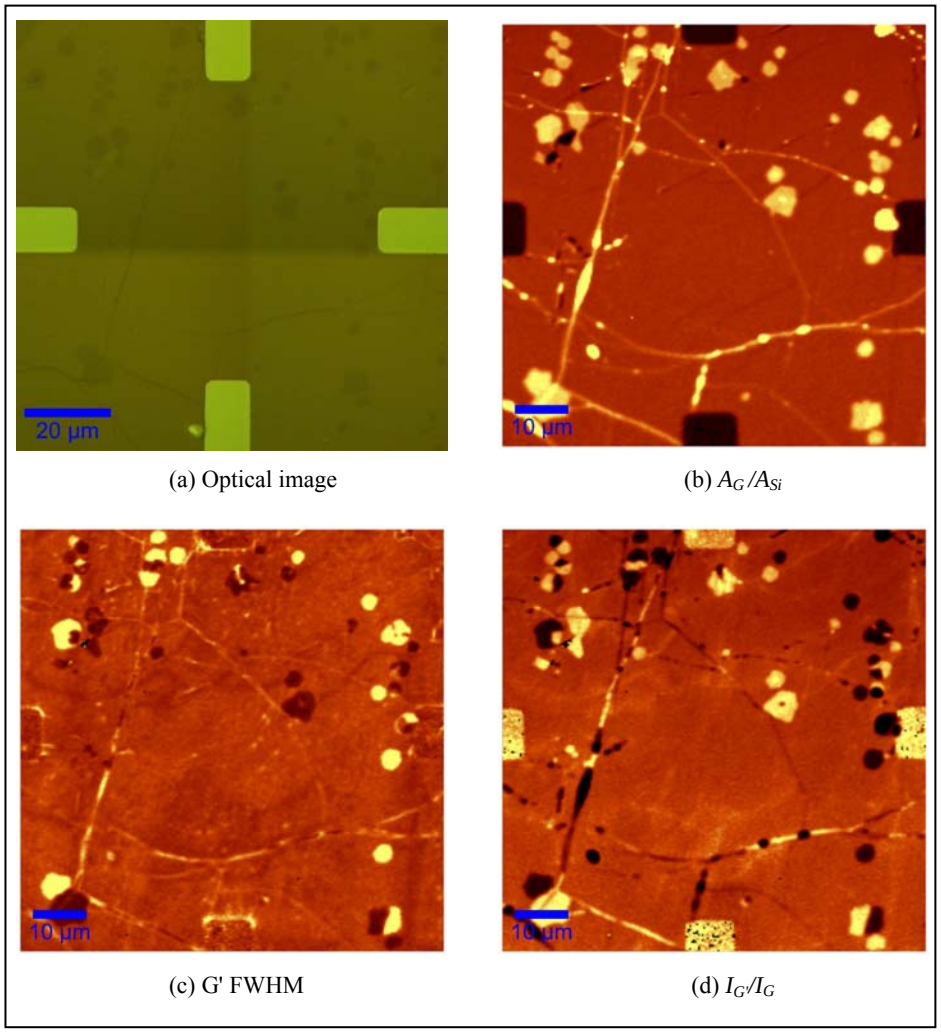

(a) Optical image (b) A_G/A_{Si}

(c) G' FWHM (d) $I_{G'}/I_G$

Figure 2. Optical and Raman images of a graphene film transferred onto patterned oxide substrate (LPC069B1TC – H_2 = 100 sccm, CH_4 = 0.5 sccm). (a) Optical image of the scanned area, Raman maps of the (b) peak area ratio A_G/A_{Si}, (c) G' FWHM, and (d) the intensity peak ratio $I_{G'}/I_G$ of the same area shown in the optical image.

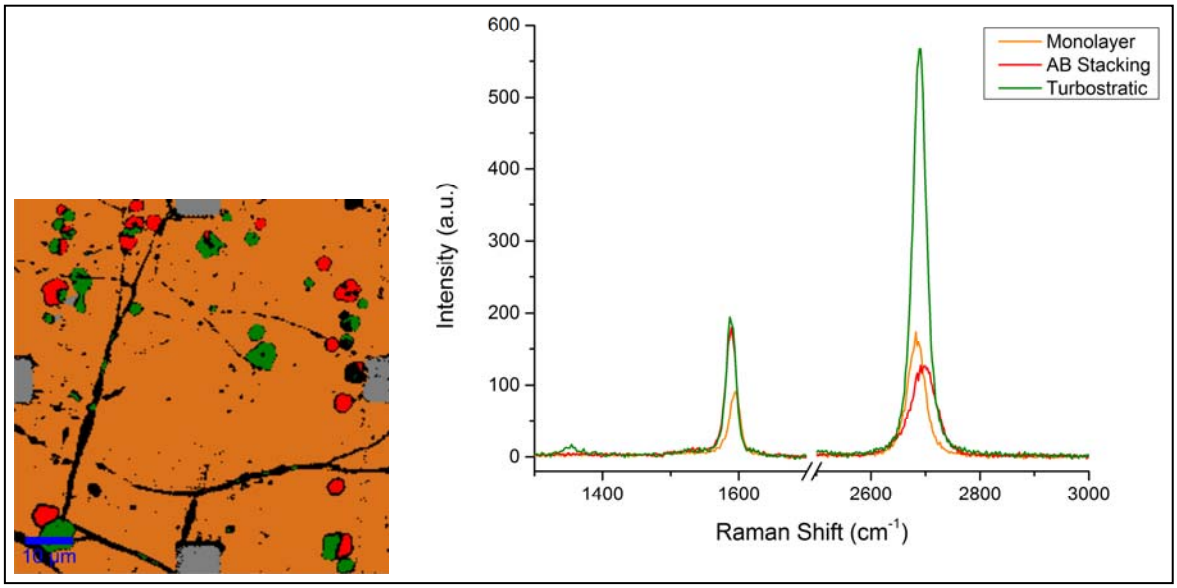

Figure 3. (a) Composite map of LPC069B1TC showing the composition of the Raman maps shown in figure 2 and (b) the corresponding Raman spectra for the three different graphene configurations—orange (SLG), red (AB-stacked bilayer), and green (turbostratic bilayer).

Representative Raman spectra for the three major compositions (SLG, AB-BLG, and T-BLG) are shown in figure 3b. The key features of the Raman spectra discussed earlier (e.g., the increased FWHM for Bernal-stacked material and differences in the G and G' peak heights) yield very distinctive spectra for each composition. Peak position shifting can also be seen for the three different configurations. A summary of the median peak position and FWHM values can be found in table 2. As expected, the G' peak position shows the most variability. The bilayer compositions show significant blue shifts from the median SLG position—7 cm^{-1} and 10.5 cm^{-1} for turbostratic and bernal stacking, respectively. The bilayer G peak position shows a smaller shift from SLG in the opposite direction (3.6–4.6 cm^{-1} red shift). Similar shifts in the position of G and G' peak have been observed in exfoliated turbostratic and AB-BLG (*12*, *14*).

Table 2. Summary of the peak fitting median values for single-layer, Bernal-stacked bilayer, and turbostratic bilayer graphene for LPC069B1TC (as seen in figure 3).

	G' Position	**G' FWHM**	**G Position**	**G FWHM**	$I_{G'}/I_G$	A_G/A_{Si}
Whole Image	2683.7	35.7	1592.4	17.0	1.8	0.14
SLG	2682.5	35.7	1592.6	17.0	1.8	0.14
AB-BLG	2693.0	56.3	1588.0	17.8	0.8	0.28
T-BLG	2689.5	29.0	1589.0	16.0	2.8	0.25

3.2 H_2/CH_4 Growth Study Results

For the films grown in this study, the $I_{G'}/I_G$ intensity map for each growth can be seen in figure 4. Two main features are observable in every Raman image. The first is the presence of folds in the graphene. It is thought that the folds more likely originate during the cool down phase of graphene growth than during the transfer process. As discussed earlier, they tend to have Raman peak characteristics that veer slightly from typical SLG and BLG values. Secondly, all images show the growths are mostly monolayer graphene with areas of bilayer graphene present. The composition of the scanned areas for each growth can be found in table 3. The values range from 83% to 93% SLG. The amounts of turbostratic and Bernal BLG varied, as well with no direct correlation to the methane flow rate. However, the size of the bilayer regions did appear to correlate with the H_2/CH_4 ratio. The average bilayer region ranged from 1 to 4 μm as the methane flow decreased (or as H_2/CH_4 increased). These results are very similar to those performed previously, where the CH_4 flow was held at 5 sccm and the H_2 flow rate was varied from 500 to 0 sccm (*15*). This suggests that the hydrogen-to-methane flow ratio plays an important role in the formation of bilayer graphene and understanding this relationship provides a pathway for producing large coverage bilayer graphene. Also noteworthly in figure 4 is the stacking of individual bilayer areas. It seems that one bilayer area or "grain" can consist of two or more different stacking configurations. For example, in the A_G/A_{Si} map of figure 2, one larger bilayer grain can be seen in the lower right hand corner and appears as one continuous area. However, both the G' FWHM and $I_{G'}/I_G$ maps show this area to have two different stacking configurations. In exfoliated graphene, two or more stacking configurations within a trilayer graphene flake has been routinely observed (*16*). However, this is not the case for exfoliated bilayer graphene. Having multiple stacking configurations in BLG is unique to CVD graphene. At this point, it is unclear as to what causes this phenomena.

Table 3. Composition of the graphene films for the H_2/CH_4 growth study based on the analysis of the Raman scanned areas.

Sample	T-BLG	AB-BLG	SLG	H_2	CH_4	H_2/CH_4
069B1TC	3.0%	1.9%	88.0%	100	0.5	200
068B1TC	3.0%	4.9%	82.5%	100	1	100
066B1TC	2.6%	3.7%	86.3%	100	2	50
067B1TC	1.9%	3.6%	85.2%	100	3	33
070B1TC	2.9%	3.7%	86.4%	100	4	25
065B1TC	1.6%	1.0%	93.0%	100	5	20

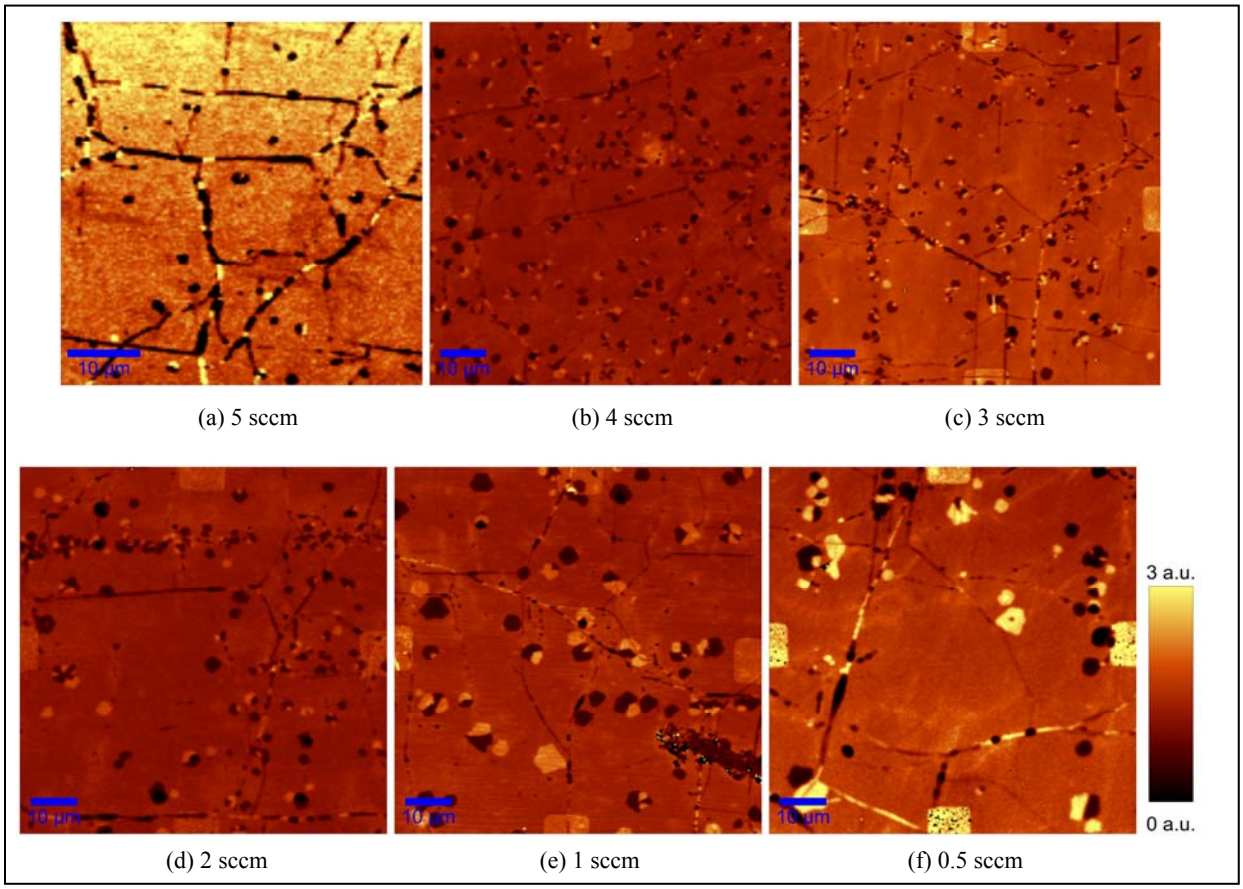

Figure 4. $I_{G'}/I_G$ peak intensity maps for the six graphene films grown with different CH_4 flow rates. The color scale shown in the figure was used for all six maps.

The quality of the graphene is typically examined by looking at the characteristic D peak. This peak arises due to symmetry breaking defects present in the graphene and is thought of as a measure for disorder with the sp^2 carbon matrix. A comparison of the D peak intensities for the growth series can be seen in figure 5. Although the intensities are quite low when compared to the G peak intensity ($I_D/I_G < 0.1$) and therefore considered good quality, correlations between areas of high D intensities and the $I_{G'}/I_G$ maps (see figure 4) can been observed. The major folds and wrinkles found in the graphene typically exhibit higher intensities of the D peak. However, most strikingly, areas that exhibit high D peak intensities are the areas that were previously identified as turbostratic or disoriented bilayer graphene. Because turbostratic BLG does not exhibit the low-energy stacking configuration, it does seem that two layers randomly oriented or rotated by one another would exhibit the symmetry breaking properties that typically give rise to the characteristics D peak. Based on this observation, it seems that the quality of the graphene should not be based solely on the presence of the D peak in the Raman spectra.

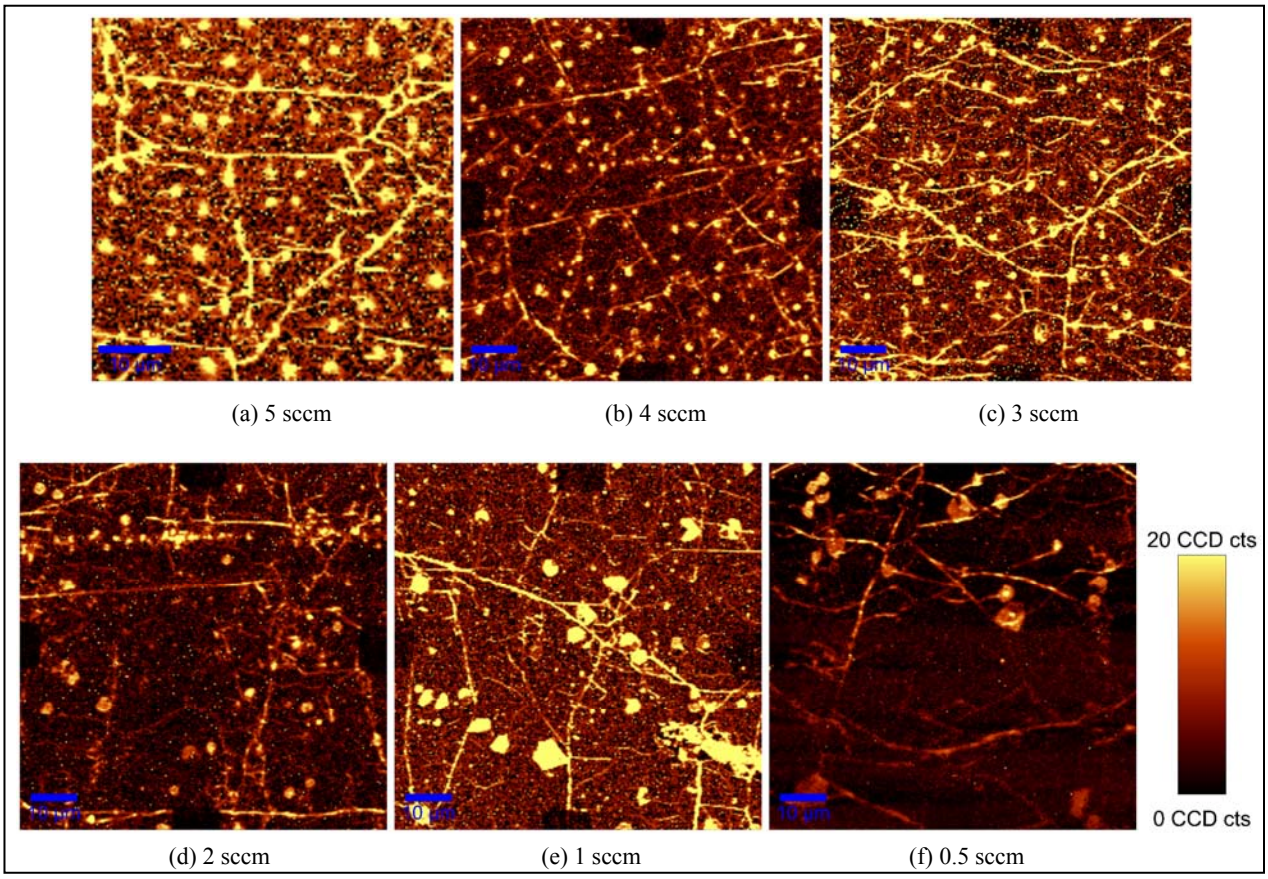

Figure 5. D peak intensity maps for the six graphene films grown under different CH_4 flow rates. The color scale shown in the figure was used for all six maps.

4. Conclusions

Raman characterization of CVD graphene grown under varying H_2/CH_4 flow ratio values was explored in this report. The growth study reveals that although the H_2/CH_4 ratio varied from 20 to 200, 100% single-layer graphene was not achieved. All growths were composed primarily of SLG with noticeable amounts of bilayer graphene present. The percentage of BLG in the graphene did not correlate with the flow ratio. However, the size of the BLG areas in each scan increased as the H_2/CH_4 increased. It should also be noted the characteristic D peak, a measure of the symmetry breaking in the sp^2 lattice, correlated to the presence of turbostratic or disoriented BLG graphene and not Bernal BLG. This analysis has proven useful to correlate growth parameters to the resulting graphene structural properties.

5. References

1. Bolotina, K. I.; Sikesb, K. J.; Jianga, Z.; Klimac, M.; Fudenberga, G.; Honec, J.; Kima, P.; Stormera, H. L. Ultrahigh Electron Mobility in Suspended Graphene. *Solid State Communications* **2008**, *146*, 351.

2. Nair, R. R.; Blake, P.; Grigorenko, A. N.; Novoselov, K. S.; Booth, T. J.; Stauber, T.; Peres, N.M.R.; Geim, A. K. Fine Structure Constant Defines Visual Transparency of Graphene. *Science* **2008**, *320*, 1308.

3. Novoselov, K. S.; Geim, A. K.; Morozov, S. V.; Jiang, D.; Zhang, Y.; Dubonos, S. V.; Grigorieva, I. V.; Firsov, A. A. Electric Field Effect in Atomically Thin Carbon Films. *Science* **2004** *306* (5696), 666–669.

4. Li, Xuesong; Cai, Weiwei; An, Jinho; Kim, Seyoung; Nah, Junghyo; Yang, Dongxing; Piner, Richard; Velamakanni, Aruna; Jung, Inhwa; Tutuc, Emanuel; Banerjee, Sanjay K.; Colombo, Luigi; Ruoff, Rodney S. Large-Area Synthesis of High-Quality and Uniform Graphene Films on Copper Foils. *Science* **2009**, *324* (5932), 1312–1314.

5. Gaskill, D. K.; Jernigan, G.; Campbell, P.; Tedesco, J. L.; Culbertsom, J.; VanMil, B.; Myers-Ward, R. L.; Eddy, Jr. C.; Moon, J.; Curtis, D.; Hu, M.; Wong, D.; McGuire, C.; Robinson, J.; Fanton, M.; Stitt, T.; Stitt, T.; Snyder, D.; Wang, X.; Frantz, E. Epitaxial Graphene Growth on SiC Wafers. *ECS Transactions* **2009**, *19*, 117–124.

6. Li, Xuesong; Cai, Weiwei; Colombo, Luigi; Ruoff, Rodney S. Evolution of Graphene Growth on Ni and Cu by Carbon Isotope Labeling. *Nano Letters* **2009**, *9* (12), 4268–4272.

7. Okamoto, H., editor. Phase Diagrams for Binary Alloys. ASM International, 2000.

8. Vlassiouk, I.; Regmi, Murari; Fulvio, Pasquale; Dai, Sheng; Datskos, Panos; Eres, Gyula; Smirnov, Sergei. Role of Hydrogen in Chemical Vapor Deposition Growth of Large Single-Crystal Graphene. *ACS Nano* **2011**, *7*, 6069.

9. Liu, Lixin; Zhou, Hailong; Cheng, Rui; Yu, Woo Jong; Liu, Yuan; Chen, Yu; Shaw, Jonathan; Zhong, Xing; Huang, Yu; Duan, Xiangfeng. High-Yield Chemical Vapor Deposition Growth of High-Quality Large-Area AB-Stacked Bilayer Graphene. *ACS Nano* **2012**.

10. Li, Xuesong; Magnuson, Carl W.; Venugopal, Archana; An, Jinho; Suk, Ji Won; Han, Boyang; Borysiak, Mark; Cai, Weiwei; Velamakanni, Aruna; Zhu, Yanwu; Fu, Lianfeng; Vogel, Eric M.; Voelkl, Edgar; Colombo, Luigi; Ruoff, Rodney S. Graphene Films with Large Domain Size by a Two-Step Chemical Vapor Deposition Process. *Nano Letters* **2010**, *10* (11), 4328–4334.

11. Petrone, Nicholas; Dean, Cory R.; Meric, Inanc; van der Zande, Arend M.; Huang, Pinshane Y.; Wang, Lei; Muller, David; Shepard, Kenneth L.; Hone, James. Chemical Vapor Deposition-Derived Graphene with Electrical Performance of Exfoliated Graphene. *Nano Letters* **2012**, *12* (6), 2751–2756.

12. Gupta, A.; Chen, G.; Joshi, P.; Tadigadapa, S.; Eklund. Raman Scattering from High-Fequency Phonons in Supported n-Graphene Layer Films. *Nano Letters* **2006**, *6* (12), 2667–2673.

13. Hwang, Jih-Shang; Lin, Yu-Hsiang; Hwang, Jeong-Yuan; Chang, Railing; Chattopadhyay, Surojit; Chen, Chang-Jiang; Chen, Peilin; Chiang, Hai-Pang; Tsai, Tsong-Ru; Chen, Li-Chyong and Chen, Kuei-Hsien. Imaging Layer Number and Stacking Order Through Formulating Raman Fingerprints Obtained from Hexagonal Single Crystals of Few Layer Graphene. *Nanotechnology* **2013**, 24 (1), 015702.

14. Poncharal, P.; Ayari, A.; Michel, T.; Sauvajol, J. L. Raman Spectra of Misoriented Bilayer Graphene. *Physical Review B* **2008**, *78* (11), 113407.

15. Dubey, Madan; Namburu, Raju; Ulrich, Marc. *Graphene-Based Nanoelectronics (Final Report)*; ARL-TR-6351; U.S. Army Research Laboratory: Adelphi, MD, 2013.

16. Lui, Chun Hung; Li, Zhiqiang; Chen, Zheyuan; Klimov, Paul V.; Brus, Louis E.; Heinz, Tony F. Imaging Stacking Order in Few-Layer Graphene. *Nano Letters* **2011**, *11* (1), 164–169.

List of Symbols, Abbreviations, and Acronyms

AB-BLG	Bernal-stacked BLG
ARL	U.S. Army Research Laboratory
BLG	bilayer graphene
CRM	confocal Raman microscope
Cu	copper
CVD	chemical vapor deposition
FWHM	full-width−half-maximum
h-BN	hexagonal boron nitride
LPCVD	Low-Pressure Chemical Vapor Deposition
Ni	nickel
PMMA	poly(methyl methacrylate)
SEM	scanning electron microscope
SLG	single-layer graphene
T-BLG	turbostratic BLG

NO. OF COPIES	ORGANIZATION
1 (PDF)	DEFENSE TECHNICAL INFORMATION CTR DTIC OCA
2 (PDFs)	DIRECTOR US ARMY RSRCH LAB RDRL CIO LL RDRL IMAL HRA RECORDS MGMT
1 (PDF)	GOVT PRINTG OFC A MALHOTRA
10 (PDFs)	DIR USARL RDRL SER P AMIRTHARAJ T KIPP RDRL SER L B NICHOLS B PIEKARSKI M DUBEY R BURKE G BIRDWELL E ZAKAR WML B R SAUSA WMM E K BEHLER

INTENTIONALLY LEFT BLANK.